Ore Geology Reviews 44 (2012) 121–135

Contents lists available at SciVerse ScienceDirect

Ore Geology Reviews

journal homepage: www.elsevier.com/locate/oregeorev

ASTER detection of chromite bearing mineralized zones in Semail Ophiolite Massifs of the northern Oman Mountains: Exploration strategy

Sankaran Rajendran [a,*], Salah al-Khirbash [a], Bernhard Pracejus [a], Sobhi Nasir [a], Amani Humaid Al-Abri [a], Timothy M. Kusky [b], Abduwasit Ghulam [c]

[a] Department of Earth Sciences, Sultan Qaboos University, Al-Khod, 123 Muscat, Oman
[b] State Key Lab for Geological Processes and Mineral Resources, Three Gorges Research Center for Geohazards, Ministry of Education China University of Geosciences, Wuhan, China
[c] Department of Earth and Atmospheric Sciences and Center for Environmental Sciences, Saint Louis University, St. Louis, MO 63103, USA

ARTICLE INFO

Article history:
Received 23 February 2011
Received in revised form 30 July 2011
Accepted 14 September 2011
Available online 18 September 2011

Keywords:
Chromites
Harzburgite
Mineralized zone
Ophiolite
Remote sensing
Semail massifs
Oman

ABSTRACT

Economically viable chromite deposit occurrences are widespread in the ultramafic rocks of Semail ophiolite massifs of the northern Oman Mountains, particularly in the basal dunite and harzburgite unit of the mantle section. Geological mapping of this region is challenging, primarily due to difficult access, complexity of structures, and lack of resolution and areal integrity of lithological differentiation using conventional mapping techniques. The present research study evaluates the discrimination and occurrence of chromites bearing mineralized zones within ophiolites by analyzing the capabilities of Landsat TM and Advanced Spaceborne Thermal Emission and Reflection Radiometer (ASTER) satellite data; using a number of selected methods including decorrelated stretching, different band rationing and Principal Component Analysis image processing techniques exist in the scientific literature. The study results show that the processed VNIR and SWIR spectral wavelength regions are promising in detecting the areas of potential chromite bearing mineralized zones within the ophiolite region, and proved to be successful for mapping of serpentinized harzburgite containing chromites. Exploration geologists, industrialists and mine owners are advised to adopt this technique and avoid the limits in filed data alone for more exploration and exploitation of areas having chromite deposits in arid region elsewhere.

1. Introduction

The Semail ophiolite of Oman (Fig. 1a) is one of the world's best and most complete examples of well-exposed ocean floor rocks (Abrams et al., 1988). It mainly consists of two main lithological units: (1) partially serpentinized mantle ultramafic rocks including harzburgite with dunite (peridotites); and (2) gabbroic–basaltic rocks from the overlying crustal section. The hot base of the Semail ophiolite developed a sole of metamorphic rocks formed at high temperature (T) and low pressure (P) during intraoceanic detachment (Bucher et al., 1988; Ghent and Stout, 1981; Searle and Malpas, 1980). At the top of the ophiolite sequence, the diabase dyke swarms (sheeted dykes) and basic extrusives – mostly spilites with pillow lava or conglomerate – occur in a sequence below the pelagic sequences (Fig. 1b).

The ultramafic rocks forming the Semail massifs contain widespread chromite mineralization (Fig. 1c) located at the Moho transition zone (MTZ) or even slightly deeper within the mantle, typically of ophiolitic podiform chromites worldwide (Li et al., 2002). Exceptional exposures are found at Wadi Fizz (Fig. 1c) located just at the boundary between the mantle and crust or 1–2 km below the Moho (Augé, 1985; Brown, 1982; Leblanc and Ceuleneer, 1992; Nicolas and Al Azri, 1991; Prichard et al., 1996a). This deposit occurs as individual lenses and varies in texture from podiform to veins. Massive chromite samples of this region have Cr_2O_3 content ranging from 31.5 to 54.61 wt.% with Cr:Fe ratio from 1.84:1 to 2.96:1 (Annells, 1989). The Platinum Group of Elements (PGE) and Platinum Group of Minerals (PGM) studies in the Oman chromites state that the chromites were formed from magma which was possibly derived from MORB-type basalt or from mantle materials (Ahmed and Arai, 2002). Large pods of chromites have also been found recently deeper within the mantle section of the Semail ophiolite massifs. The chromites are economically valuable. There are several open cast mining operations that are ongoing over the region. The discrimination of mantle ultramafic harzburgite with dunite (partially serpentinized) rocks and delineation of the areas of potential chromite mineralized zones within the Semail ophiolite massifs in this region are of great importance (Eckstrand, 1984; Evans, 1980).

Due to the extent of the area (1169 km^2) and extremely rugged topography, with elevations between 0 and 2500 m, exhaustive sampling and detailed mapping are impossible. Remote sensing is able to provide more detailed mapping of the areas of chromite mineralized zones in the ultramafic section of the ophiolite and it facilitates the exploration geologists, industrialists and mine owners for cost saving exploitation. Remote sensing is most suitable technique to apply in arid regions like Oman where there are rock exposures over the surface and no vegetation

* Corresponding author. Tel.: +968 24142249.
E-mail address: sankaranrajendran@yahoo.com (S. Rajendran).

0169-1368/$ – see front matter © 2011 Elsevier B.V. All rights reserved.
doi:10.1016/j.oregeorev.2011.09.010

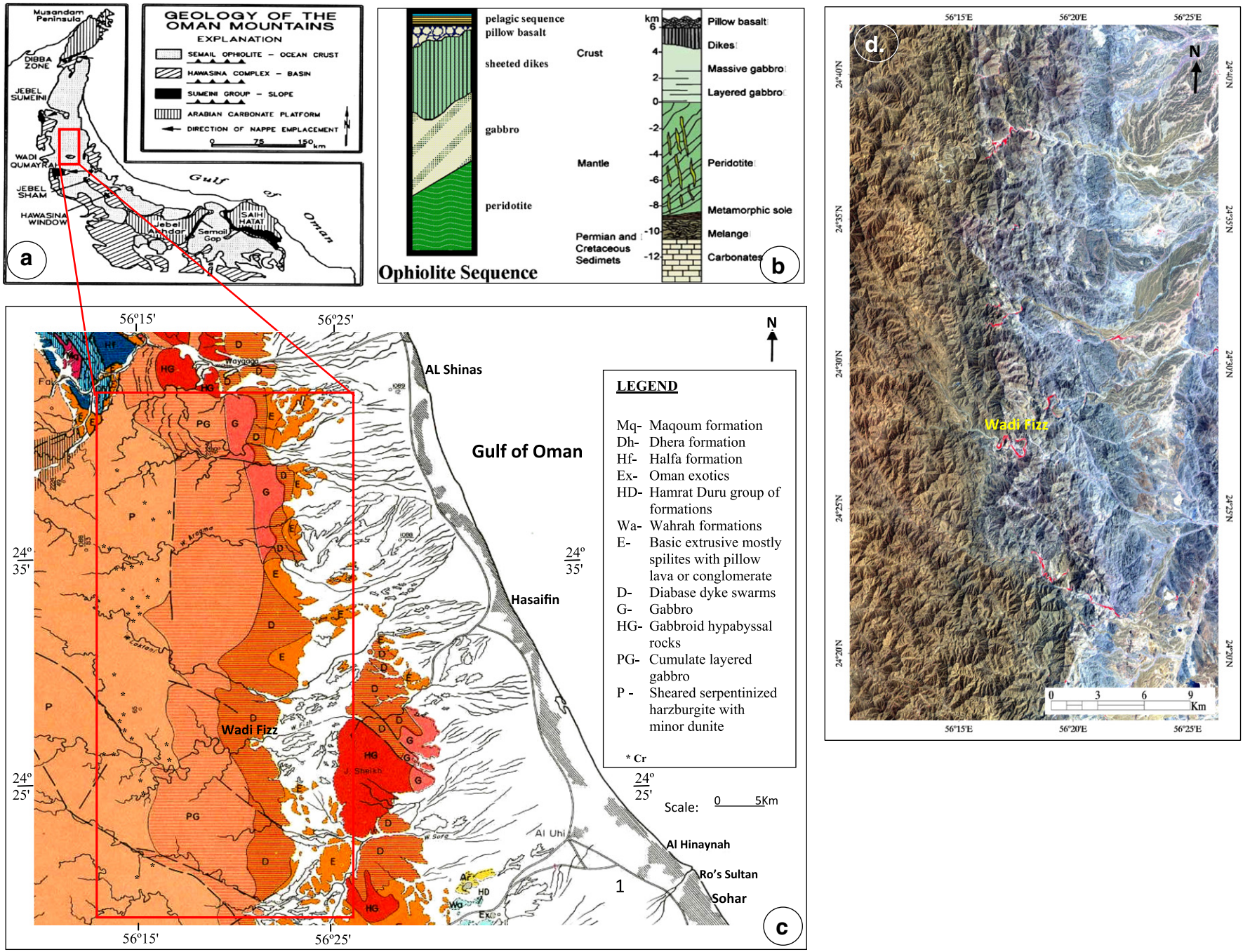

Fig. 1. a. Geology of Oman Mountain (after Watts, 1990) showing the locations of b. Ophiolite Sequence, c. geology (Source: Ministry of Petroleum and Minerals, 1987) and d. ASTER RGB (3,2,1) image of study area.

disturbance (Fig. 1d). Abrams (1986), Rothery (1987a) and Abrams et al. (1988) have previously outlined the level of apparent lithological discrimination of the Oman ophiolite possible with Landsat Thematic Mapper (TM) images. The ASTER bands and their longer wavelength regions allow discrimination between wide ranges of mineral compositions and lithologies. For example, the ASTER band combination 7-3-1 which is equivalent to Landsat ETM 7-4-2 is used to distinguish between granitic rocks in the southern and western parts of the image of the Wadi Kid metamorphic belt (Abdeen et al., 2001). Gad and Kusky (2006) used ASTER band ratios image (4/7, 4/6, 4/10) for mapping the granite and metamorphic belt of the Wadi Kid area of Sinai, Egypt. They concluded that these band ratios can be used for mapping metamorphic rocks in the Arabian Nubian Shield and other arid regions. The six SWIR bands (with 30-m spatial resolution) are useful for soil, and lithological mapping, and in characterization of the absorption features of phyllosilicates and carbonate minerals (e.g., Yamaguchi and Naito, 2003). The five TIR bands (10–14) have 90 m spatial resolution and their emissivity spectra are used to characterize silicate rocks (Yamaguchi et al., 1998). In this paper, we delineated the area of chromites bearing mineralized zone by analyzing the capability of the Advanced Spaceborne Thermal Emission and Reflection Radiometer (ASTER) sensor image evaluated along with the Landsat TM image by taking the advantage of visible near infrared (VNIR) and short wavelength infrared (SWIR) reflectance properties of the ophiolite lithologies and incorporating our field observations. Essentially, the decorrelated stretching, different band rationing and Principal Component Analysis (PCA) image processing techniques previously published in scientific publications on mapping of ophiolites are used to delineate the area of potential chromite bearing mineralized zones occurring in ophiolitic rocks of the Semail ophiolite massifs of the northern mountain region of Oman. The results are discussed to show how image processing techniques can selectively highlight the rock harzburgite with dunite and the area of potential chromite mineralized zones to recommend the techniques to the exploration geologists, industrialists and mine owners avoiding their ambiguity on more exploration and exploitation of similar deposits in the arid region. We suggest that the satellite data interpretations are adequate for producing lithological maps at 1:100,000 scale and can show many details more appropriate to mapping at 1:50,000 or better (Abrams et al., 1988). The study area we here illustrate was mapped in different degrees of detail some years earlier by the Ministry of Petroleum and Minerals (1987) of Oman.

2. Geology

The emplacement of Semail ophiolite massifs of northern mountain region of Oman onto the Arabian plate during the Late Cretaceous is now well documented and generally agreed upon (Boudier et al., 1985; Coleman, 1981; Glennie et al., 1973, 1974; Lippard et al., 1986; Searle and Malpas, 1980). Numerous studies that detail the igneous and structural history of the Semail ophiolite as well as the stratigraphy of the Oman continental margin have clarified the evolution and passive nature of this margin during the Permian to Late Cretaceous period. The geometry and nature of the continental margin bounding the Arabian carbonate platform in the area of the Oman Mountains were disrupted during the Late Cretaceous Oman orogeny. Extensive thrust sheets (nappes) of the Semail Ophiolite and Hawasina Complex cover most of the Arabian carbonate platform margin except at the major tectonic windows at the Musandam Peninsula, Jebel Akhdar, and Saih Hatat (Glennie et al., 1973, 1974; Fig. 1a). In detail, the Semail ophiolite in Oman (SE Arabia) is a 600 km long by up to 150 km wide slab of Cretaceous oceanic crust and mantle emplaced due to closure of the Tethyan Ocean. This closure can be related to an earlier fundamental change in plate motion between Africa and Eurasia (Boudier et al., 1985; Dercourt et al., 1986; Moores et al., 1984). During the Aptian, the movement of the African plate changed from an eastward direction to a northward one and by the Campanian it had rotated nearly 63° — counterclockwise relative to Eurasia (Dercourt et al., 1986). The eastern passive margin of Oman experienced crustal thickening in the Early Cretaceous as a fragment of Gondwanaland moved northward causing transpression and possibly colliding with that margin. Divergence of the oceanic crust in the Tethys at a spreading center to the NE of the Oman margin (Boudier et al., 1985) initiated the obduction of the Semail ophiolite by gravity sliding across the subsiding passive continental margin. Later uplift of the Oman mountains in the Tertiary and Quaternary has been related to the ongoing collision between Arabia and Eurasia (Kusky et al., 2005).

The study area (Fig. 1c), west of Al Shinas-Hasaifin-Sohar region is located in the Semail ophiolite massifs which are parallel to the East Coast of the Gulf of Oman (which includes Wadi Aragma, Wadi Laktani, Wadi Fish and Wadi Jizzi). The rocks consist of strongly sheared harzburgite with dunite (P), cumulate layered gabbro (PG), gabbroid hypabyssal rocks (HG), gabbro (G), diabase dyke swarms (D) and basic extrusives which are mostly spilites with pillow lavas or conglomerate (E) of Middle Cretaceous age. The exposures of Wahrah formations (Wa), Hamrat Duru group of formations (HD), Oman exotics (Ex), Halfa formation (Hf), Dhera formation (Dh) and Maqoum formation (Mq) occur in the NW and NE parts of the area (Fig. 1c) as Post-Nappe Allochthonous Units belonging to late Tertiary to Quaternary age. The ophiolitic metagabbros in the area are closely associated with other ophiolitic members' i.e., harzburgite and metabasalts. The mafic–ultramafic transition zone in the Semail ophiolite is located in between the top of the strongly sheared harzburgite (with dunite) tectonic unit and the base of the continuous layered gabbro unit. The Moho is in the upper horizon of the transition zone where dunites become interlayered with lenses of gabbro, themselves grading into the continuous layered gabbro unit (Nicolas and Prinzhofer, 1983). The two most important features of the transition zone are, (1) it is rich in dunites. Downwards, these dunites root into the harzburgites following a vein pattern which is more or less transposed into a lenticular transition. Upwards, they form a continuous unit below the layered gabbros. (2) It is rich in chromite pods, either discordant or concordant with respect to the foliation inherited from asthenospheric flow (Cassard et al., 1981) located within the transition zone. Small scale detailed geological mapping shows the occurrence of chromites in this area. The field investigation and searching of mining areas in 'Google Earth' confirm the presence of several mines that are active at several places in the area.

3. Satellite data

To better discriminate the harzburgites and the area of chromite bearing mineralized zones within the transition zone, a comparative study is performed between Landsat TM and ASTER spectral bands. The TM instrument carried by the Landsat satellite records data in seven multispectral bands including six channels in the visible and reflected infrared part of the electromagnetic spectrum and one channel in the thermal infrared. The Landsat TM data used in this study was acquired on March 4, 2003 with 0% cloud cover. The ASTER sensor onboard the Earth Observing System (EOS) TERRA platform is a multispectral imaging system, launched in December 1999, which travels in a near circular, sun-synchronous orbit with an inclination of approximately 98.2°, an altitude of 705 km and a repeat cycle of 16 days. This contribution uses 14-band ASTER Level 1B data acquired on April 18, 2006. The imagery is supplied in terms of scaled radiance at-sensor data with radiometric and geometric corrections applied. It is georeferenced in the UTM projection and for the WGS-84 ellipsoid. The sensors characteristics and the wavelength regions of both the instruments are given in Table 1 The increase of spectral bands in the ASTER SWIR region (one spectral band for Landsat versus six spectral bands for ASTER) enhances the surface lithological mapping capability.

4. Spectral characteristics of ophiolites and chromite

Several authors utilized remote sensing and GIS techniques for lithological mapping as well as identifying mineral deposits (Abrams and Hook, 1995; Abrams et al., 1983; Gad and Kusky, 2007; Gabr et al., 2010; Kusky and Ramadan, 2002; Mars and Rowan, 2006; Rowan and Mars, 2003; Rowan et al., 2003; Sabins, 1997). Hunt (1977) stated that remote sensing is of valuable use in mapping of hydrothermally altered minerals that have distinct absorption features. Sabins (1997) demonstrated that remote sensing is a valuable tool for mineral exploration in at least four ways: 1) mapping regional lineaments and structural trends along which groups of mining may occur, 2) mapping local fracture patterns that may control individual ore deposits, 3) detecting hydrothermally altered rocks associated with ore deposits, and 4) providing basic geologic data. In addition to the synoptic coverage provided by remote sensing, another major advantage of the technique is the use of reflectance properties beyond the visible range of the spectrum to discriminate rock types. The reflectance spectrum of a rock depends on the mineralogical composition of its surface, which is usually a mixture of the whole rock mineralogy and weathering minerals. Absorption in bands in the visible and short wavelength infrared can rise due to either electronic or vibrational processes that occur in these minerals. Earlier spectral reflectance studies provide important insights to the causes of spectral variations for the interpretation of optical remote sensing data (e.g., Cloutis and Gaffey, 1991; Cloutis et al., 2004). Abrams et al. (1988) presented a detailed review about ophiolite lithology derived from Hunt and Salisbury (1970), Hunt et al. (1974) and Hunt (1977). The laboratory reflectance spectra indicative of the range of spectral features produced by some of the ophiolite minerals which may dominate weathered surfaces discussed by Abrams et al. (1988) are shown in Fig. 2. It includes spectra collected from two unweathered ophiolite lithologies as examples of the idealized spectral response, which in reality is partly or completely masked by that of the weathering minerals. Serpentinite shows a relatively flat spectral response. The shallow feature at 0.45 μm is due to ferric iron and the broader absorption centered near 0.9 μm or around 1.0 μm is due to ferrous iron. The rather sharp band at 2.3 μm is due to vibrational processes of Mg–OH, and hydration effects are shown by the absorption near 1.4 μm. The harzburgite spectrum has a broad feature attributable to ferrous iron in pyroxene and olivine minerals, centered near 1.0 μm (Abrams et al., 1988).

In general, the electronic processes in the minerals include three types, viz. conduction bands, charge transfer and crystal field effects. The presence of ferrous iron (Fe^{2+}) in weathered surface produces

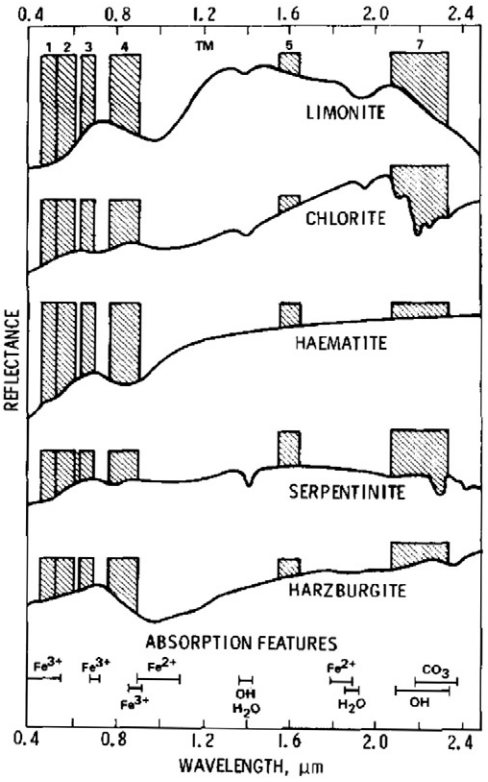

Fig. 2. Reproduced from Abrams et al. (1988) showing the laboratory spectral reflectance measurement of some minerals and rocks important in remote sensing of ophiolites, with the Landsat TM band passes. Spectra are included from coarse particulate samples: hematite, chlorite and serpentinite data of Abrams et al. (1988); limonite is from Hunt et al. (1971); and harzburgite is from Hunt et al. (1974).

absorptions centered at about 0.45 μm, 1.0–1.1 μm, 1.8–1.9 μm, and 2.2–2.3 μm, depending on its lattice environment. The ferric iron (Fe^{3+}) produces absorptions at about 0.65 μm and 0.87 μm. The vibrational processes which cause visible and short-wavelength infrared absorptions are bending and stretching vibrations of bonds within radicals or molecules. On igneous rock surfaces, the most important are due to Al–OH and Mg–OH in clays, micas, amphiboles and serpentine. Al–OH produces absorptions centered at about 2.2 μm, whereas Mg–OH produces features at about 2.3 μm. There are features in the infrared due to vibrations within molecular

Table 1
Sensor characteristics of Landsat TM and ASTER instruments.

Sensors	Landsat TM	ASTER		
Characteristics		VNIR	SWIR	TIR
Spectral bands with range (μm)	Band 1 0.45–0.52	Band 01 0.52–0.60 Nadir looking	Band 04 1.6–1.7	Band 10 8.125–8.475
	Band 2 0.52–0.60	Band 02 0.63–0.69 Nadir looking	Band 05 2.145–2.185	Band 11 8.475–8.825
	Band 3 0.63–0.69	Band 03N 0.76–0.86 Nadir looking	Band 06 2.185–2.225	Band 12 8.925–9.275
	Band 4 0.76–0.90	Band 03B 0.76–0.86 Backward looking	Band 07 2.235–2.285	Band 13 10.25–10.95
	Band 5 1.55–1.75 Band 610.40–12.50 Band 7 2.08–2.35		Band 08 2.295–2.365 Band 09 2.36–2.43	Band 14 10.95–11.65
Spatial Resolution (m)	30	15	30	90
Swath width (km)	180	60	60	60
Radiometric Resolution (bits)	8	8	8	12
Cross track Pointing		±318 km (±24 deg)	±116 km (±8.55 deg)	±116 km (±8.55 deg)

water (Abrams et al., 1988; Rajendran et al., 2011). Cloutis et al. (2004) stated that the Cr content has the depth of the absorption band near 0.55 μm. The best correlations exist between Cr content and wavelength positions at 0.49, 0.59, 2, 17.5, and 23 μm in the absorption bands. In this study, the iron ion presence in the mafic and ultramafics is probably responsible for all the detectable bands. The highly sheared and weathered harzburgite (having more serpentine) of the Semail ophiolite can be discriminated by a simple color composition at 0.45 μm (green), 0.9 or 1.0 μm (red) and 2.3 μm (blue) which may yield as harzburgite in green and dunite in yellow colors and the discrimination of harzburgite having chromites may show a very sharp contact with other crustal lithologies.

5. Methodology

To delineate the area of chromite potential mineralized zone and host harzburgite of the study area, the advantage of the visible and short wavelength infrared reflectance properties of the ophiolite lithologies is taken and studied over Landsat TM and ASTER satellites images. The decorrelated stretching, different band rationing and principal component analysis image processing techniques tested in scientific publications on mapping of ophiolite are used. In final stages, the field validation is carried out and the results are incorporated. In this study, the regional geological map is used to support the remote sensing studies.

Decorrelation stretching is becoming a widely used technique, as discussed by Gillespie et al. (1986), Rothery (1987a,b) and Abrams et al. (1988). It is based on a principal component transformation of the acquired data. Here, the transformed channels can themselves be contrast stretched and arbitrarily assigned primary colors for display as a color composite image. Abrams et al. (1988) mapped the Oman ophiolite using enhanced Landsat Thematic Mapper data by the processing of decorrelation stretching and confirmed that the data have the capacity to capitalize on distinctions in the spectral reflectance of different rock types and their weathering products. Further, they stated that the decorrelation stretching of these data produces images (RGB: 7, 5 and 4) capable to recognize variations in gabbro composition and to identify small acidic, gabbroic and ultramafic intrusions. A similar method is attempted here to discriminate the harzburgite and chromite bearing mineralized zones using Landsat TM data.

The band ratio images are used to suppress the topographic variation and the image brightness difference related to grain size variation (Adam and Felic, 1967; Sultan et al., 1987). This technique has been used successfully in lithological mappings for the Arabian Nubian Shield and for other areas worldwide (Abrams et al., 1983; Amer et al., 2010; Gabr et al., 2010; Galvao et al., 2005; Goetz et al., 1983; Kruse et al., 1993; Matthews and Jones, 1992; Ninomiya et al., 2005; Ramadan et al., 2001; Rowan et al., 2003; Sultan et al., 1987; Swayze et al., 1998). Band selection for the different ratio images used is based on the spectral signatures of rocks. When rationing techniques are applied, all the reasonable grouping of minerals of such rocks is best discriminated by a combination of ratios that includes short wavelength bands (i.e. 3/1, 4/1 or 4/2), the ratio of the long wavelength bands (5/ 7) and a ratio of one band each from short and long wavelength band groups (e.g., 5/4 or 5/3) (Crippen, 1989). Such ratio images designed to display the spectral contrast of specific absorption features can be used extensively in geological remote sensing (Rowan et al., 1974, 1977). For the discrimination of harzburgite (contains more serpentine) rocks and chromite bearing mineralized zones of the study area, using Landsat TM satellite data, the RGB band ratios used to discriminate serpentinites by Sultan et al. (1986) (5/7, 5/1, 5/4×4/3), Sabins (1999) (3/5, 3/1, 5/7) and Gad and Kusky (2006) ((5/3, 5/1, 7/5) and (7/5, 5/ 4, 3/1)) are used. They stated that these band ratios can be used to discriminate serpentinites of ophiolites having high amounts of magnetite and hydroxyl-bearing minerals from the surrounding mafic rocks in the arid regions.

Considering the spectral information in the VNIR and SWIR wavelength portions, ASTER data represents an enormous innovation in terms of their improved spectral characteristics and higher spatial resolution (e.g., Abdeen et al., 2001; Bedell, 2001; Hewson et al., 2001; Okada and Ishii, 1993; Rajendran et al., 2011; Rowan and Mars, 2003; Rowan et al., 2003; Velosky et al., 2003). The minerals and rocks having diagnostic spectral features in this wavelength range include iron oxides, phyllosilicates (clay minerals), sulfates and carbonates among others (Crósta and Filho, 2003; Crosta and Moore, 1989). ASTER band-ratio combinations and band math are effective in emphasizing spectral characteristics of certain rocks and minerals and discriminating harzburgite of ophiolites (Abdeen et al., 2001; Bedell, 2001; Hewson et al., 2001; Okada and Ishii, 1993; Rowan and Mars, 2003; Rowan et al., 2003; Velosky et al., 2003). For better mapping of harzburgite and to delineate the area of chromite potential mineralized zone in the ophiolites of the study region, we used here the potential of VNIR and SWIR regions of ASTER data and ASTER band rationing and Principal Component Analysis (PCA) image processing techniques which have also been commonly applied to Landsat Thematic Mapper (TM) data to locate hydrothermal alteration zones and related to metallic deposits (Amer et al., 2010; Gabr et al., 2010; Podwysockii et al., 1983). The ASTER band ratio images (4/7, 4/1, 2/3×4/3) and (4/7, 3/4, 2/1) were used by Abdeen et al. (2001) for mapping ophiolites, metasediments, volcaniclastics, and granitoids lithologic units of the Neoproterozoic Allaqi Suture in southern Eastern Desert of Egypt. Amer et al. (2010) constructed the ASTER band ratios ((2+4)/3, (5+7)/6, (7+9)/8) by summing the bands representing the shoulders of absorption features as a numerator, and the band located nearest the absorption feature as a denominator to discriminate between different ophiolitic and granitic rocks in a Red–Green–Blue (RGB) color combination and identified the ophiolitic rocks, metagabbros, and metabasalts. They stated that the ratio is much better than the previously published ASTER band ratios. Thus, the above discussed band ratio combinations were applied to the study area.

In the PCA technique, the relationship between the spectral responses of target minerals or rocks and numeric values extracted from the eigenvector matrix is used to calculate the Principal component images. Using this relationship, one can determine which PCs contain the spectral information due to minerals and whether the digital numbers (DNs) of pixels containing the target minerals had high (bright) or low (dark) values (Crósta and Filho, 2003; Crósta and Moore, 1989; Loughlin, 1991; Rokos et al., 2000). A PCA is applied to the 9 ASTER bands (e.g., Richards and Xiuping, 1998) of study area. The pre-treatment and processing of ASTER images for above said techniques are followed as stated in Abdeen et al. (2001) and Amer et al. (2010). It is generally accepted that the first three high order principal components (1, 2, and 3) have over 99% of the spectral information; hence these have been widely used for lithological mapping rather than the subsequent low order principal components (4, 5, 6, etc.) which usually contain less than 1% of spectral information and they contain low signal-to-noise ratios. However, some of the higher order principal components provide subtle information about the occurrence of mineral and rock types that are spatially dominant in the image. It is also interesting to use a combination of certain lower order components which takes up some of the information with higher order principal components to highlight some target spectral signatures (Amer et al., 2010).

6. Results and discussion

6.1. Discrimination of ophiolites and delineation of chromite mineralized zone

6.1.1. Landsat TM mapping

Understanding the spectral absorption characters of the rocks of ophiolites and chromites (Abrams, 1986; Rothery, 1987a) as outlined

above, the Landsat TM and ASTER satellite data of the study area was processed using the discussed methodologies and now we are able to validate and better define the distribution of harzburgites with dunites and the area of occurrence of chromite mineralized zones within ophiolites by incorporation of our field observations and observed evidence from 'Google Earth'. We are confident that the lithological discrimination revealed by the imagery is sufficiently uniform throughout the ophiolite and can be used as a reliable mapping criterion.

The decorrelated image processed using the three infrared bands (TM bands 7, 5 and 4) displayed in red, green and blue (comparable to Abrams et al., 1988) given in Fig. 3 contains Band 4 information relating to the presence of iron; Band 5 characterizes the general albedo of the materials to highlight certain altered (ferric iron-bearing) rocks which have particularly high reflectances near 1.6 μm, whereas ferrous iron can cause depression of the reflectance curve in this region and Band 7 responds to the presence of hydroxyl-bearing minerals by a reduction in reflectance due to various hydroxyl- and H,O-related features. The decorrelated image shows almost all ophiolite rock types which are discriminated and separable in distinct colors comparable to the geology map (Fig. 1c). They are: (1) the mantle sequence (the strongly sheared serpentinized harzburgite with dunite) of Oman appears in two distinct color units (Abrams et al., 1988) including the upper part running about 1 km below the Moho, which is usually a purple color on the image (CD), not mapped on geology map (Fig. 1c) and most of the rest of the mantle sequence appears in a dark green-yellow color (P); (2) the harzburgite with gabbro intrusions (PG) appears from cyan through to greenish-yellow due to reflecting differences in mafic content; (3) the high-level gabbros (G) are most often yellow in color; (4) the diabase (D) often appears as pink areas

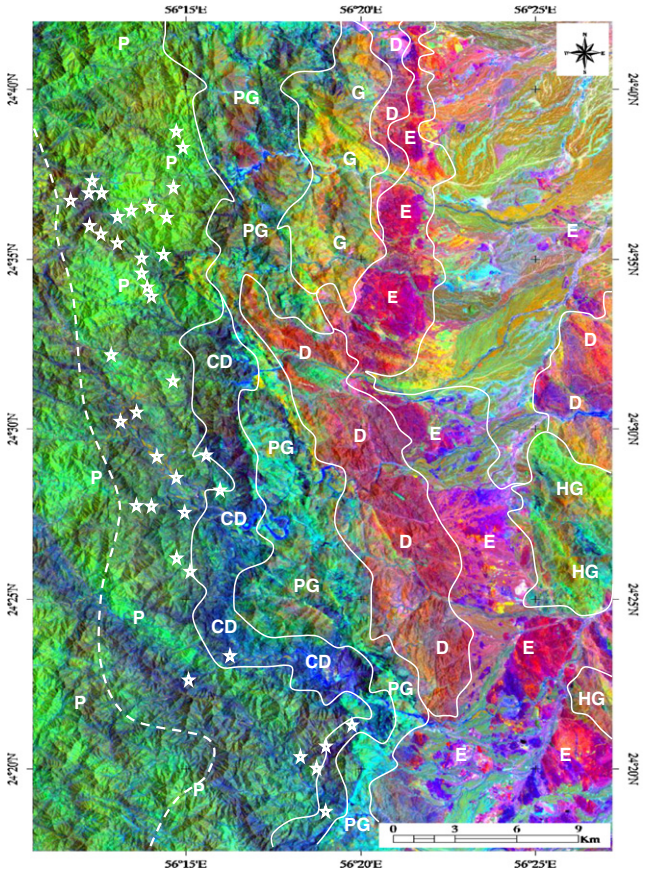

Fig. 3. Landsat TM RGB (7, 5, 4 bands) decorrelated image of study area (Abrams et al., 1988). The abbreviations of the image are E — Basic extrusives mostly spilites with pillow lava or conglomerate; D — Diabase dyke swarms; G — Gabbro; HG — Gabbroid hypabyssal rocks; PG — Cumulate layered gabbro; P and CD — Sheared serpentinized harzburgite.

but shows a variety of colors due to variable degrees of iron oxide and hydroxide coating and differences in primary mineralogy (Abrams et al., 1988); and (5) the basic extrusives (E) typically appears orange to red, and lavas appear mostly magenta. Areas which are especially affected by chloritic–epidotic alteration (notably within sheeted dykes and upper parts of the gabbros) tend to appear orange, due to strong ferric iron absorption in band 4, resulting in a degree of ambiguity in lithological interpretation (Abrams et al., 1988).

The dark color absorption of region (CD) in the boundary between dark green-yellow color showing strongly sheared serpentinized harzburgite (tectonized) (P) and yellow color showing gabbro (PG) is due to presence of iron oxides (or variable percentages in mafic elements). We interpret the area of potential chromite mineralized zones within mantle sequences (the area of purple color: upper part (CD) and dark green-yellow color: lower part (P), Fig. 3) below the Moho (line separating PG) to run about 1 to 5 km (up to dashed line) based on image interpretations and acquired evidence on the occurrences of chromites (star marked) available in the geological map (Fig. 1c) and the identified chromite mines in the 'Google Earth' image (Fig. 4; http://www.google.com/earth/index.html). The geographical locations of possible occurrences of chromite mines identified on Google Earth are given in Table 2 and Fig. 4. Almost all chromite mines fall within the area of strongly sheared serpentinized harzburgites (near to upper mantle sequences). The location of chromite and mine occurrences and the mineralized zone are delineated with the spatial accuracy of 4 to 5 pixels on Landsat TM image that is having approximately less than 150 mts.

The images produced by band ratios of Sultan et al. (1986) (5.7, 5/1, 5/4×4/3), Sabins (1999) (3/5, 3/1, 5/7) and Gad and Kusky (2006) ((5/3, 5/1, 7/5) and (7/5, 5/4, 3/1)) for the study area are given in Fig. 5a, b, c and d. These can be studied with the decorrelated RGB image (Fig. 3) and geology (Fig. 1c). The RGB band ratio images of Sultan et al. (1986) and Sabins (1999) show the serpentinized harzburgite in dark green-yellow color owing to the absorption by MgO- and OH-bearing minerals. The area of mineralized zone delineated from Moho in bright red color is due to the high degree of absorption of iron bearing minerals, as described by Sultan et al. (1986). In the Sabins (1999) ratio, the zone appears violet-yellow in color. The RGB band ratio images (5/3, 5/1, 7/5 and 7/5, 5/4, 3/1) of Gad and Kusky (2006) show the serpentinized harzburgites in a dark violet-bluish color that depends on the chosen band combinations. The images show the area of chromite mineralized zone in dark purple (3/5, 3/1, 5/7 and 5/3, 5/1, 7/5) and pink (7/5, 5/4, 3/1) colors. However, the zone is easily interpretable on the image produced by Sultan et al. (1986) due to high brightness existing in red color. The other ophiolitic rock types of the study area processed by the discussed band ratios can be compared and studied with geology (Fig. 1c) of the area. Over all the Landsat TM RGB band ratio images processed based on the above combinations proved as very effective in discriminating serpentinized harzburgites and delineating the area of chromites bearing mineralized zones of study area.

6.1.2. ASTER mapping

The image spectral reflectance or the spectra derived from the ASTER reflectance image for the major rock units similar to the study area such as serpentinized harzburgites, gabbros and metabasalts are well discussed and evaluated using USGS spectral library by Amer et al. (2010). Their results show that serpentine which is the main component of serpentinized harzburgites has two absorption features at 1.4 and 2.35 μm. Gabbros and metabasalts consist mainly of pyroxene with an absorption feature at 2.35 μm, anorthitic plagioclase has two absorption features around 2 and 2.4 μm, and olivine has absorption features between 0.8 and 1.2 μm.

The ASTER band ratios (4/7, 4/1, 2/3*4/3; Fig. 6a) of Abdeen et al. (2001) are equivalent to the Landsat TM image (5/7, 5/1, 3/4*5/4; Fig. 5a) of Sultan et al. (1986) and the ASTER band ratio image (4/7,

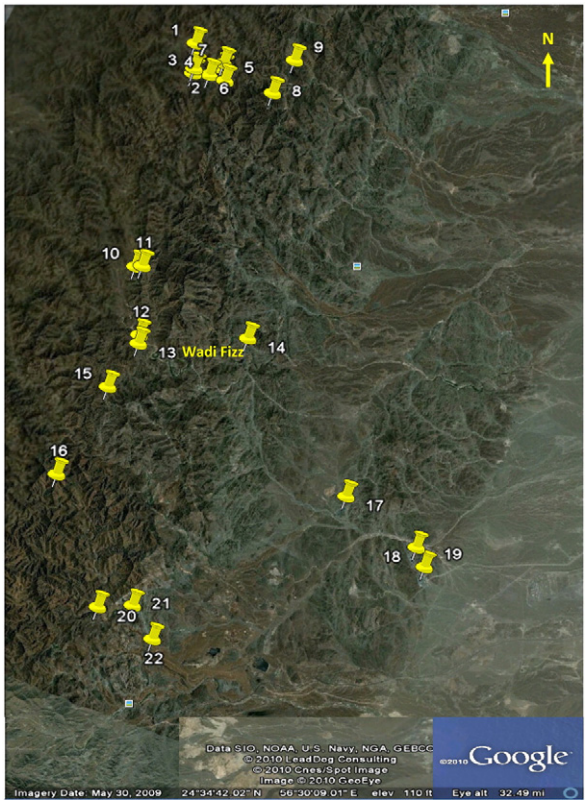

Fig. 4. Google Earth map of part of study area shows the locations of chromite mines.

3/4, 2/1; Fig. 6b) of Abdeen et al. (2001) is equivalent to the Landsat TM image of Abram's combination (5/7, 4/5, 3/1), well developed to highlight clay, and hydroxyl and iron oxide minerals are used by (Abdeen et al., 2001) for mapping serpentinite, granite and marble lithologic units of the Neoproterozoic Allaqi Suture in the southern Eastern Desert of Egypt. The image processed on band ratio (4/7, 4/1, 2/3*4/3) and (4/7, 3/4, 2/1) of study area shows the serpentinized harzburgites in brown-yellowish and green-pinkish colors. The area of mineralized zone is well discriminated in red-pinkish color by the band ratio (4/7, 4/1, 2/3*4/3) however, the contact between the serpentinized harzburgites with other ophiolitic rocks is not well discriminated.

Recently, Amer et al. (2010) used image spectra as a reference and produced a new ASTER band ratio ((2+4)/3, (5+7)/6, (7+9)/8) using the band absorption features, where the numerator is the sum of the bands representing the shoulders, and the denominator is the band located nearest the absorption feature minimum taken for mapping of ophiolites (serpentinites, metagabbros, and metabasalts) and granites of Central Eastern Desert of Egypt and suggested the ratio is best for lithological mapping in arid regions. Here, the band ratio (2+4)/3 highlights the serpentinites and metabasalts, (5+7)/6 highlights the granitic rocks, and (7+9)/8 highlights the metagabbros and serpentinites. These band ratios were used by them in red, green and blue to produce a color image to distinguish between serpentinites from the other ophiolitic rocks. Since the present study is focused on discriminating the serpentinized harzburgites and taking advantage of these combinations, here we applied this technique to the study area to discriminate the serpentinized harzburgites from other ophiolite rock units and to delineate the area of chromite mineralized zone. The geologic interpretations of ASTER band ratios ((2+4)/3, (5+7)/6, (7+9)/8) image (Fig. 6c) shows the sharp contact of serpentinized harzburgites between other ophiolitic rocks well.

In Principal Component Analysis of ASTER bands, the image of the first five components is given in Fig. 7 where, the PCA 2nd component (Fig. 7b) highlights the serpentinized harzburgites, the PCA 4 (Fig. 7d) highlights the basic gabbros and the PCA 5 component (Fig. 7e) shows some interesting signatures on the post tectonic younger metabasalts, the extrusives. Thus, we selected these three bands (PC5, PC4, and PC2) for better discrimination of serpentinized harzburgites among the other ophiolitic rocks (gabbros, and metabasalt) and for delineation of the area of potential chromite mineralized zone (Amer et al., 2010). The RGB results of PC5, PC4 and PC2 comparable to Amer et al. (2010) is given in Fig. 8. The geologic interpretations of the image show that the highly sheared serpentinized harzburgites (mantle sequences) are discriminated by pink color (CD: upper part of sequence) and greenish yellow (P: lower part of sequence) from gabbros which have red-orange colors, and metabasalts which have dark blue colors. The area of potential chromites bearing mineralized zone is delineated more clearly from pink and greenish yellow colors within the serpentinized harzburgites with the spatial accuracy of 2 to 3 pixels on ASTER image which is having approximately less than 50 mts. The gabbro intrusions and associated rock units are also well discriminated within ophiolite rocks, better than the band ratio image. The image shows that the PCA is powerful in distinguishing the subtle differences between the various rock units of the study area.

Table 2
Shows the geographical positions of locations of chromites mines.

No	Latitude	Longitude
1	24°27′6″N	56°12′59″E
2	24°36′18″N	56°13′21″E
3	24°36′8″N	56°13′23″E
4	24°36′18″N	56°13′55″E
5.	24°36′20″N	56°14′33″E
6.	24°36′40″N	56°14′15″E
7.	24°36′53″N	56°14′11″E
8.	24°36′38″N	56°16′15″E
9.	24°37′59″N	56°16′23″E
10.	24°29′13″N	56°14′44″E
11.	24°29′21″N	56°14′57″E
12.	24°27′7″N	56°15′58″E
13.	24°26′50″N	56°16′5″E
14.	24°28′32″N	56°19′29″E
15.	24°25′3″N	56°15′50″E
16.	24°21′36″N	56°15′41″E
17.	24°24′53″N	56°25′17″E
18.	24°24′15″N	56°28′25″E
19.	24°23′44″N	56°29′1″E
20.	24°17′55″N	56°19′7″E
21.	24°18′26″N	56°20′12″E
22.	24°17′38″N	56°21′24″E

6.2. Field interpretation

To evaluate the VNIR and SWIR regions of Landsat TM and ASTER satellite data and discriminate ophiolitic rocks and the area of chromite bearing mineralized zones, during November–December 2010, we carried out field-checks on Semail ophiolite massifs with existing geological maps and interpreted satellite images. In almost all cases, our fieldwork confirmed in showing real lithological information and detection of area of chromite bearing mineralized zones by the interpreted remote sensing imagery.

In the field, the Semail ophiolite massifs of study area (Fig. 9a) covers the most complete ophiolite succession and comprises highly sheared serpentinized harzburgites (Fig. 9b), layered gabbro (Fig. 9c), diabase dykes (Fig. 9d) and pillow basalt exposed from the upper mantle to the upper crust (Johnson et al., 2004). There are several wadis (i.e., valleys) cutting the ophiolite from west to east downstream, which provide excellent exposures of rocks with which to examine the whole section. The ophiolite has virtually no soil or vegetation cover

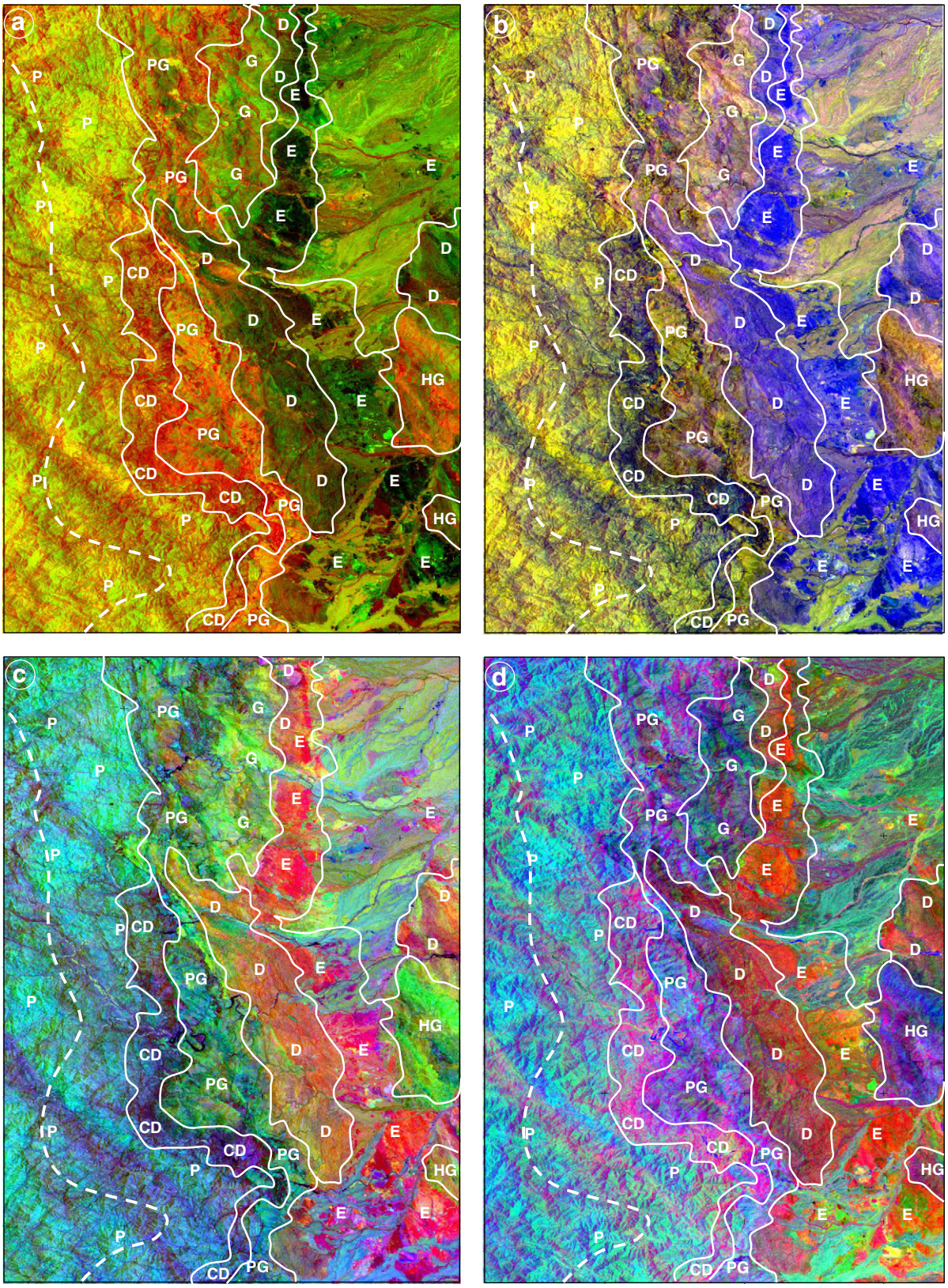

Fig. 5. Landsat RGB band ratio image a. Sultan et al., 1986 (5/7, 5/1, 5/4×4/3), b. Sabins, 1999 (3/5, 3/1, 5/7) and c. and d. Gad and Kusky, 2006 (5/3, 5/1, 7/5) and (7/5, 5/ 4, 3/1) of the study area. The abbreviations of the image are E — Basic extrusives mostly spilites with pillow lava or conglomerate; D — Diabase dyke swarms; G — Gabbro; HG — Gabbroid hypabyssal rocks; PG — Cumulate layered gabbro; P and CD — Sheared serpentinized harzburgite.

and forms rugged mountainous terrain at elevations mostly between 500 and 1500 m (Fig. 9a). Exposure of the rocks is excellent, though there is often a large amount of virtually in situ debris which hinders precise mapping of specific contacts. The ophiolite contains a complete ophiolite sequence from tectonized and variably serpentinized harzburgite (the mantle sequence), passing upwards into layered cumulate

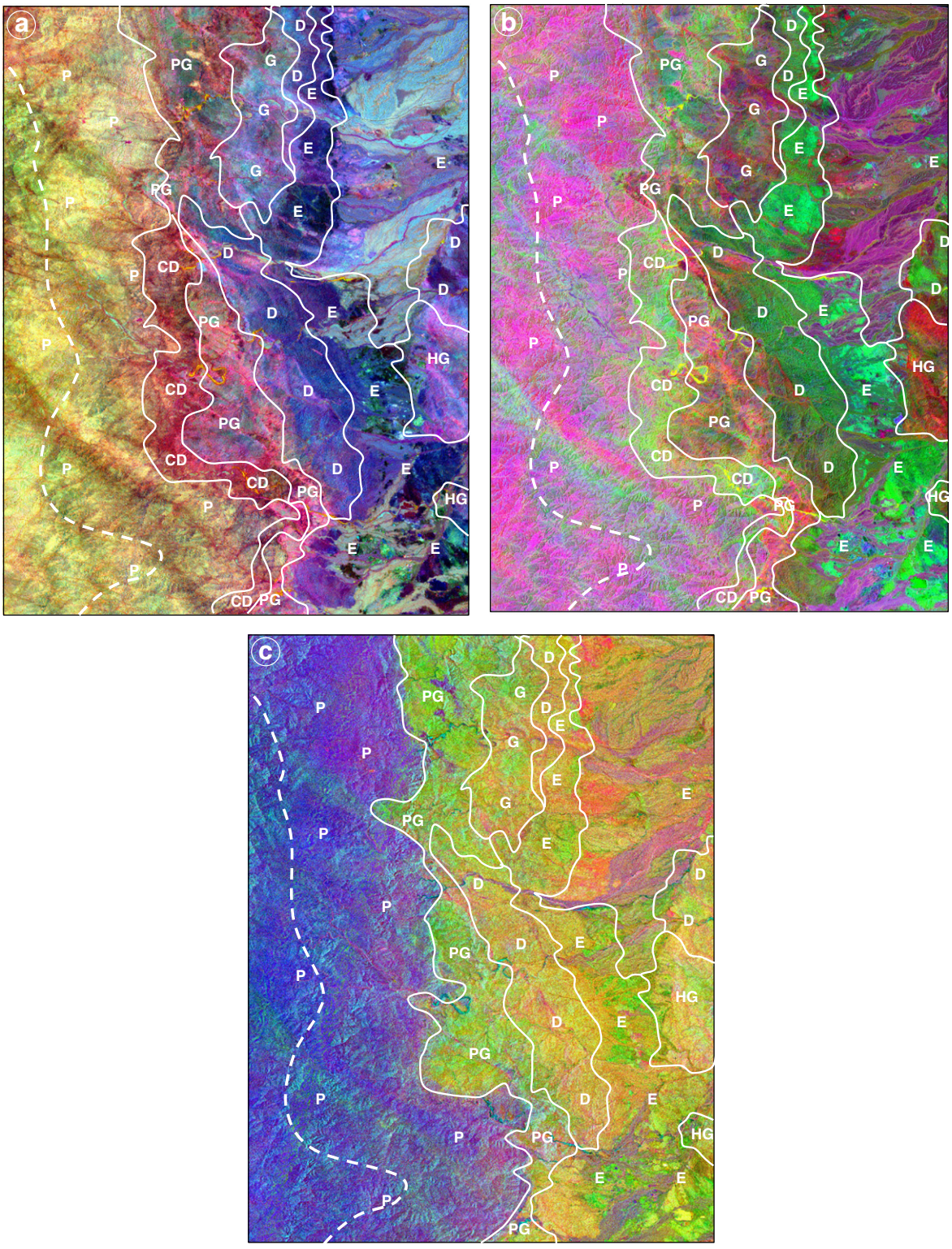

Fig. 6. ASTER RGB band ratios image a. Abdeen et al., 2001 (4/7, 4/1, 2/3*4/3) b. (4/7, 3/4, 2/1) and c. Amer et al., 2010 ((2+4)/3, (5+7)/6, (7+9)/8) of the study area. The abbreviations of the image are E — Basic extrusives mostly spilites with pillow lava or conglomerate; D — Diabase dyke swarms; G — Gabbro; HG — Gabbroid hypabyssal rocks; PG — Cumulate layered gabbro; P and CD — Sheared serpentinized harzburgite.

gabbro and diabase dyke swarms and pillow lavas fed from the magma chambers. It is intruded by post-tectonic later mafic dykes that cut almost all of the Semail ophiolite units. The mantle section consists mainly of pervasively foliated, highly tectonized and weathered harzburgite with minor amounts of dunite, chromite and basal lherzolite (Lippard et al., 1986). Dunite is predominant over harzburgite in the uppermost part of the mantle forming the Moho transition zone (CD in Figs. 3, 5, 6 and 8). More serpentine is observed in serpentinite formations and the associated gabbro body is relatively poor in serpentine.

The harzburgites are deeply affected by hydrothermal processes. The weathered harzburgites are traversed by numerous magnesite veins (Fig. 9b, e). In hand specimen, fresh harzburgite is fine to

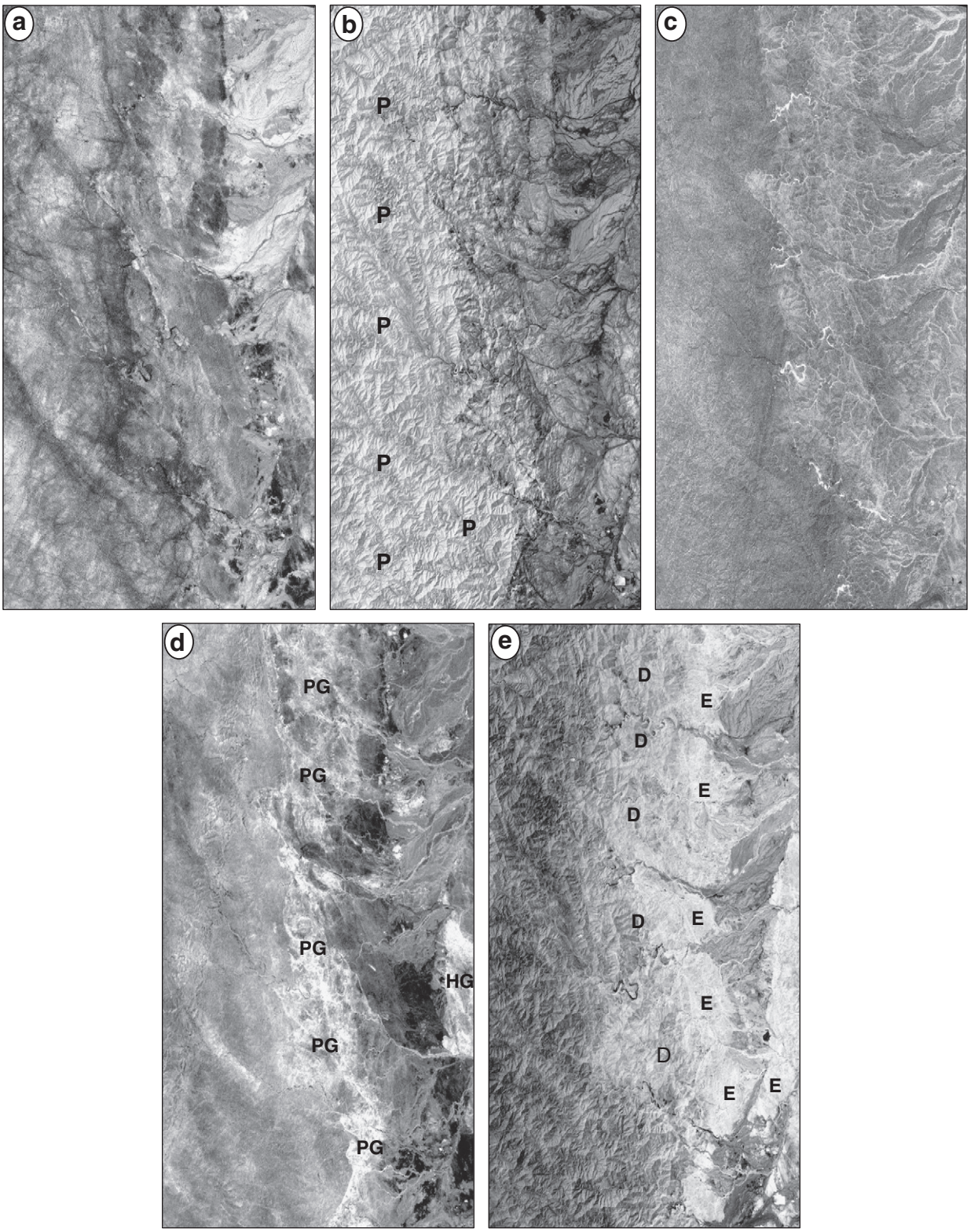

Fig. 7. (a–e). PC1 to PC5 of PCA bands of the study area. The abbreviations of the image are E — Basic extrusives mostly spilites with pillow lava or conglomerate; D — Diabase dyke swarms; HG — Gabbroid hypabyssal rocks; PG — Cumulate layered gabbro; P — Sheared serpentinized harzburgite.

medium-grained, massive and greenish gray in color (Fig. 9b). The oxidized harzburgite attains reddish to brownish color with a gradational contact with the fresh serpentinite (Fig. 9e). Also, cauliflower, fine-grained and massive magnesite is recorded cementing wadi sediments over large areas. The magnesite occurs as fine to medium grains and is usually stained with iron oxides along grain boundaries. These were formed by weathering of serpentinite under the action of CO_2-rich surface and ground water. Field study shows that the occurrence of chromite veins are in serpentinized harzburgite (Fig. 9e, f). In hand specimens, chromites are present as disseminated grains or podiform bodies. Metagabbros form an elongate body that displays layering on a regional scale (Fig. 9c), where coarse-grained

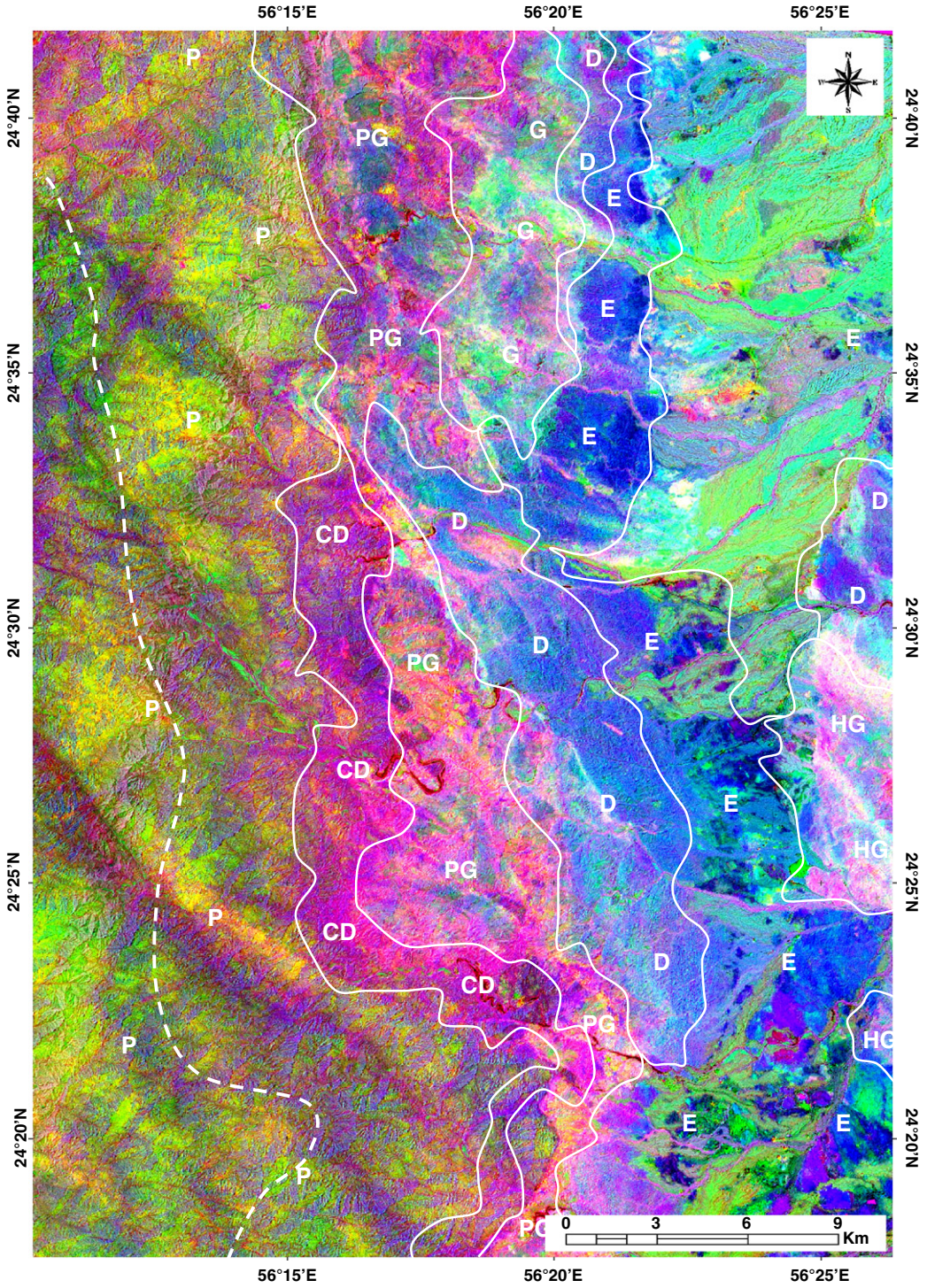

Fig. 8. RGB image of PC7, PC5 and PC4 of PCA bands of the study area. The abbreviations of the image are E — Basic extrusives mostly spilites with pillow lava or conglomerate; D — Diabase dyke swarms; G — Gabbro; HG — Gabbroid hypabyssal rocks; PG — Cumulate layered gabbro; P and CD — Sheared serpentinized harzburgite.

metagabbros are located at the base of the mountain and then grade upward to medium-grained rocks at intermediate level and are fine-grained at the top. The metagabbro contact with the serpentinites is highly sheared and mylonitized. In well preserved ophiolite sections, the layering in the basal layered gabbros is parallel to the surface separating them from the tectonized harzburgites.

Following our fieldwork, we are now confident to state here that the color distinctions revealed by decorrelation stretching, different band rationing and PCA of the satellite data are well correlated with ophiolite lithology and have a direct meaning in terms of the petrology of the rocks and the surfaces. This enables us to check the boundaries of rock units existing on the maps and discriminating the serpentinized harzburgites and more mafic and less mafic gabbros. It also facilitates to locate the Moho within ophiolites. On the imagery, the color change from yellow through green to cyan on the enhanced imagery represents increasing mafic content of serpentinized harzburgites. Many gabbroic and ultramafic late-intrusive bodies were identified parallel to mineralized zone within the ophiolite massifs. In the field,

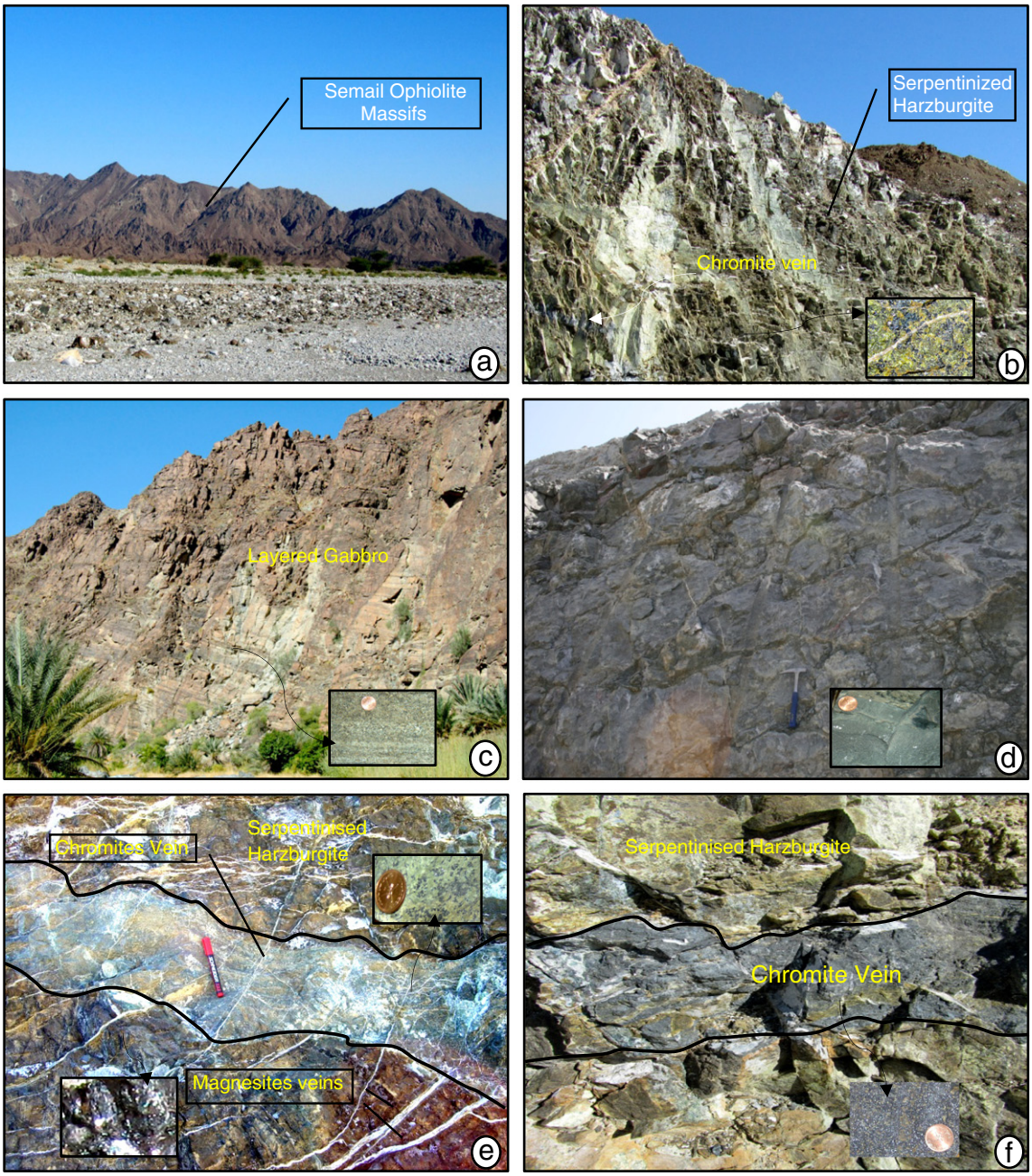

Fig. 9. Field photographs show (a) Semail ophiolite massifs and the major ophiolite rock units namely (b) serpentinized harzburgite (c) layered gabbro and (d) meta basalts. Occurrence of (e) fracture filled magnesite and (f) chromite veins within harzburgite is observed in the shear zone near Wadi Fizz.

this area is found to consist of rhythmically-layered (cumulate) and unlayered (high-level) gabbro and a hitherto unrecognized belt of sheeted dykes. The ophiolitic metabasalts in the area are exposed as an elongate body and thrust over the serpentinites. The occurrence of the mineralized zone below the Moho runs about 1–5 km interpreted from above discussed image processing techniques with spatial accuracy of approximately less than 150 mts on Landsat TM and 50 mts on ASTER satellite data is confirmed by the field work. The ophiolitic rock formations interpolated on the Google Earth map (Fig. 10) show that the identified mining areas fall within the interpreted shear zone and the zone parallel to Moho. Further, the field interpretations confirm the occurrence of area of chromite mining areas more in folded areas occurring in between the strongly sheared serpentinized harzburgites and gabbro.

Fig. 6c clearly discriminates the sharp contact between the "purple" mantle and the Moho suggesting that the causes may be related to hydrothermal alteration or serpentinization that occurred in serpentinized harzburgites. The hydrothermal alteration extends at least as deep as the base of the crust through fractures. In Fig. 8, the purple color shown perpendicular to the Moho is due to late-stage fractures in the mantle and interpreted as a post-emplacement serpentinization effect (Rothery, 1987a,b).

7. Conclusions

In this study, the Landsat TM and ASTER satellite data processed in VNIR and SWIR spectral wavelength regions allow discrimination of ophiolite lithologies (harzburgite, metagabbro, and metabasalt). The

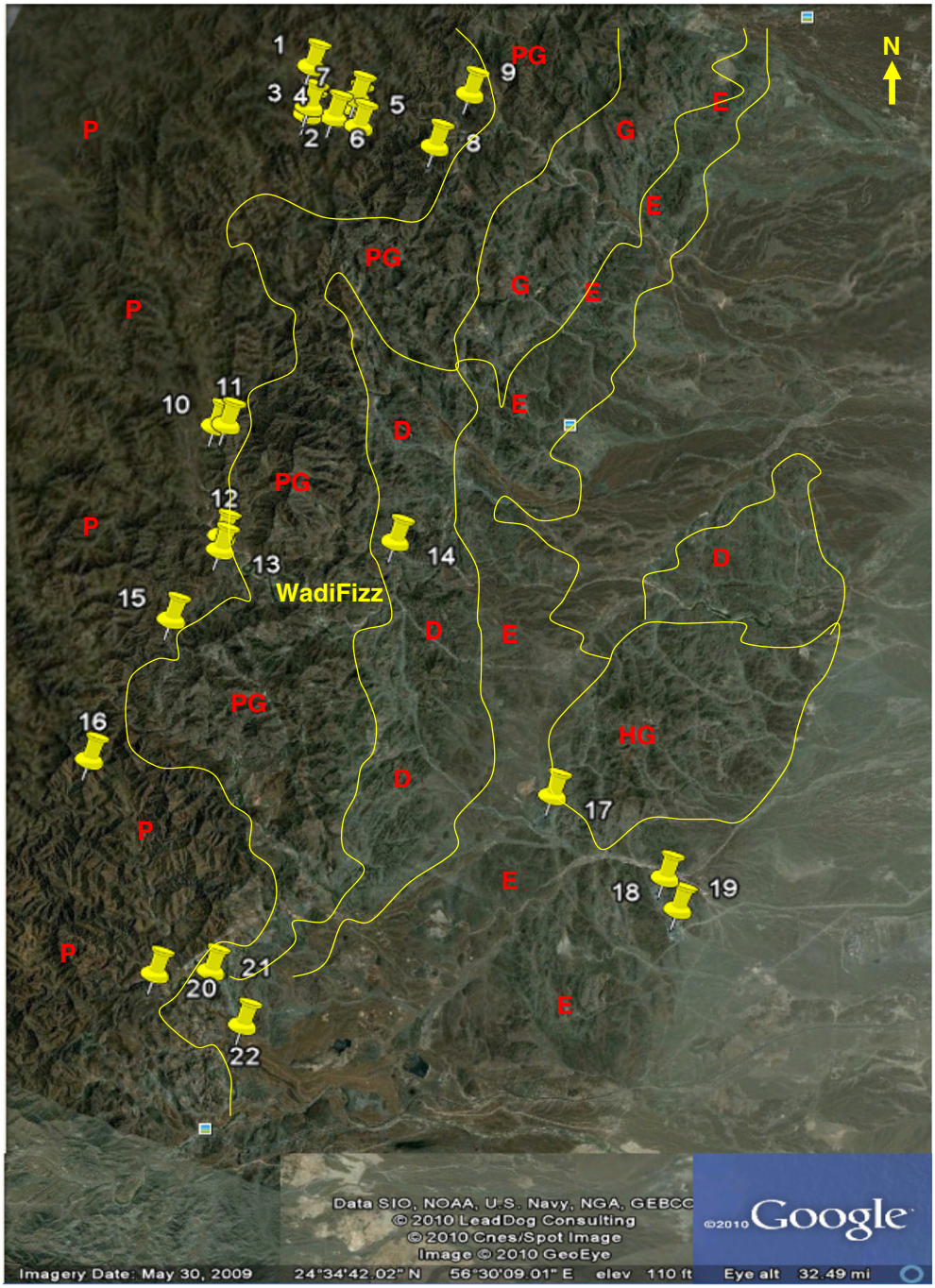

Fig. 10. Google Earth map of part of study area shows the locations of chromite mines with boundaries of different ophiolite rocks interpreted visually.

delineation of the chromite-bearing mineralized zone of Semail ophiolite massifs of northern mountain region of Oman by decorrelation stretching, band ratios and principal component analysis proved successful in discrimination of ophiolite lithologies and delineation of the area of chromite mineralized zone within ophiolites of the study area. Comparison of results of processed images derived from the methods exists in the scientific literatures, and evidence acquired from 'Google Earth' and through field work validated and confirmed the occurrence of chromite mineralized zone below the Moho run about 1 to 5 km within mantle sequences. The study suggests that the discussed techniques have potential, as time- and cost-effective methods, for mineral exploration targeting additional chromite deposits in comparison to the time consuming classical field mapping and exploration, especially in inaccessible areas.

Acknowledgments

The authors are thankful to NASA Land Processes Distributed Active Archive Center User Services, USGS Earth Resources Observation and Science (EROS) Center (https://LPDAAC.usgs.gov) for providing the ASTER data. Additional funds were provided by the National Natural Science Foundation of China (Grants 91014002, and 40821061) and the Ministry of Education of China (B07039). The help extended by Abdulla Al-Fahdi, Chief Technician, Department of Earth Sciences, Sultan Qaboos University is thankfully acknowledged. The transport facility extended by SQU to carry out field check in rugged Semail ophiolite massifs is thankfully acknowledged. The authors are sincerely thanking the anonymous reviewers for their constructive comments and suggestions.

References

Abdeen, M.M., Allison, T.K., Abdelsalam, M.G., Stern, R.J., 2001. Application of ASTER band-ratio images for geological mapping in arid regions; the Neoproterozoic Allaqi Suture, Egypt. Geol. Soc. Am. Abstr. Program 3 (3), 289.

Abrams, M.J., 1986. Mapping the Oman ophiolite using TM data. Proceedings, Thematic Conference on Remote Sensing for Exploration Geology (Reno, Nevada, 29 September-2 October, 1986). Environment Research Institute, Ann Arbor, MI, pp. 85–95.

Abrams, M.J., Hook, S.J., 1995. Simulated ASTER data for geologic studies. IEEE Trans. Geosci. Remote Sens. 33, 692–699.

Abrams, M.J., Brown, D., Lepley, L., Sadowski, R., 1983. Remote sensing for porphyry copper deposits in southern Arizona. Econ. Geol. 78, 591–604.

Abrams, M.J., Rothery, D.A., Pontual, A., 1988. Mapping in the Oman ophiolite using enhanced Landsat Thematic Mapper images. Tectonophysics 151, 387–401.

Adam, J.B., Felic, A.L., 1967. Spectral reflectance 0.4–2.0 micron of silicate rock powders. J. Geophys. Res. 72, 5705–5715.

Ahmed, A.H., Arai, S., 2002. Unexpectedly high-PGE chromitite from the deeper mantle section of the northern Oman ophiolite and its tectonic implications. Contrib. Mineralog. Petrol. 143, 263–278.

Amer, R., Kusky, T.M., Ghulam, A., 2010. New methods of processing ASTER data for lithological mapping: examples from Fawakhir, Central Eastern Desert of Egypt. J. Afr. Earth Sci. 56 (2–3), 75–82.

Annells, A.N., 1989. Exploration for Chromite in the Fizh, Far Far-Hilti and Shik Areas of Northern Oman. The Robertson Group plc, p. 25. report no 4364.

Augé, T., 1985. Platinum-group mineral inclusions in ophiolitic chromitite from the Vourinos complex, Greece. Can. Mineralog. 23, 163–171.

Bedell, R.L., 2001. Geological mapping with ASTER satellite: new global satellite data that is a significant leap in remote sensing geologic and alteration mapping. Special Publication, vol. 33. Geological Society of Nevada 329–334.

Boudier, F., Bouchez, J.L., Nicolas, A., Cannat, M., Ceulleneer, G., Misseri, M., Montigny, R., 1985. Kinematics of oceanic thrusting in the Oman ophiolite: model of plate convergence. Earth Planet. Sci. Lett. 75, 215–222.

Brown, M.A., 1982. Chromite Deposits and Their Ultramafic Host Rocks in the Oman Ophiolite. Ph.D. thesis, Open Univ., Milton Keynes, U.K.

Bucher, J., Kurz, D., Peters, T.J., Stoessel, F., Ziegler, U., 1988. The metamorphics below the Semail nappe in the northern Oman Mountains. The Geology and Tectonics of the Oman Region; A discussion meeting. Edinburgh, p. 12. Abstracts.

Cassard, D., Nicolas, A., Rabinowicr, M., Moutte, h., Leblanc, M., Prinxbofer, A., 1981. Structural classification of chromite pods in southern New Caledonia. Econ. Geol. 76, 805–831.

Cloutis, E.A., Gaffey, M.J., 1991. Pyroxene spectroscopy revisited: Spectral-compositional correlations and relationship to geothermometry. J. Geophys. Res. 96, 22809–22826.

Cloutis, E.A., Sunshine, J.M., Morris, R.V., 2004. Spectral reflectance–compositional properties of spinels and chromites: Implications for planetary remote sensing and geothermometry. Meteorit. Planet. Sci. 39, 545–565.

Coleman, R.G., 1981. Tectonic setting for ophiolite obduction in Oman. . Geophys. Res. 86, 2497–2508.

Crippen, R.E., 1989. Selection of Landsat TM band and band-ratio combinations to maximize lithologic information in color composite displays. Proceedings, 7th Thematic Conference on Remote Sensing for Exploration Geology II, pp. 912–921.

Crósta, A.P., Filho, C.R.S., 2003. Searching for gold with ASTER. Earth Obs. Mag. 12 (5), 38–41.

Crosta, A.P., Moore, MCM, J., 1989. Enhancement of Landsat Thematic Mapper imagery for residual soil mapping in SW Minas Geris State Brazil: a prospecting case history in greenstone belt terrain. Proceedings of the 9th Thematic Conference on Remote Sensing for Exploration Geology, Calgary (Ann. Arbor, MI: Environmental Research Institute of Michigan), pp. 1173–1187.

Crosta, A.P., DE Souza Filho, Brodie, A.F., 2003. Targeting key alteration minerals in epithermal deposits in Patagonia, Argentina, using ASTER imagery and principal component analysis. Int. J. Remote sens. 24, 4233–4240.

Dercourt, J., Zonenshain, L.P., Rlcou, L.E., Kazmin, V.G., Le Pichon, X., Knipper, A.L., Grandjacquet, C., Sbori-Shikov, J.M., Gevssant, J., Lepvr-Er, C., Pechersky, D.H., Boulin, J., Sibuet, J.C., Savostin, L.A., Sorokhtin, O., Westphal, M., Bazhenov, M.L., Lauer, J.P., Bhu-Duval, B., 1986. Geological evolution of the Tcthys from the Atlantic to the Pamirs since the Lias. Tectonophysics 123, 241–315.

Eckstrand, O.R., 1984. Canadian mineral deposit types: a geological synopsis. Economic Geology Report 36. Ottawa: Geological Survey of Canada.

Evans, A.M., 1980. An Introduction to Ore Geology. Blackwell, London.

Gabr, S., Ghulam, A., Kusky, T., 2010. Detecting areas of high-potential gold mineralization using ASTER data. Ore Geology Reviews 38, 59–69.

Gad, S., Kusky, T.M., 2006. Lithological mapping in the Eastern Desert of Egypt, the Barramiya area, using Landsat thematic mapper (TM). J. Afr. Earth Sci. 44, 196–202.

Gad, S., Kusky, T.M., 2007. ASTER spectral ratioing for lithological mapping in the Arabian-Nubian shield, the Neoproterozoic Wadi Kid area, Sinai, Egypt. Gondwana Res. 11 (3), 326–335.

Galvao, L.S., Filho, R.A., Vitorello, I., 2005. Use of ASTER short-wave infrared bands for the spectral discrimination of hydrothermally altered-materials: evaluation in a tropical savannah environment. Anais XII Simposio Brasileiro de ensoriamento remote, Goiania, Brazil. INPE 1783–1787.

Ghent, E.D., Stout, M.Z., 1981. Metamorphism at the base of the Samail ophiolite, Oman. J. Geophys. Res. 86, 2557–2571.

Gillespie, A.R., Kahle, A.B., Walker, R.E., 1986. Color enhancement of highly correlated images. 1. Decorrelation and HSI contrast stretches. Remote Sens. Environ. 20, 209–735.

Glennie, K.W., Boeuf, M.G.A., Hughes Clarke, M.W., Moody-Stuart, M., Pilaar, W.F.H., Reinhardt, B.M., 1973. Late Cretaceous nappes in the Oman Mountains and their geologic significance. Am. Assoc. Petrol. Geol. Bull. 57, 5–27.

Glennie, K.W., Boeuf, M.G.A., Hughes-Clarke, M.W., Moody-Stuart, M., Pilaar, W.H.F., Reinhardt, B.M., 1974. Geology of the Oman Mountains. Verhandelingen van het Koninklijk Nederlands geologisch mijnbouwkundig Genootschap: Delft, 31, p. 423.

Goetz, A.F.H., Rock, B.N., Rown, L.C., 1983. Remote sens. explor.: An overview: Econ. Geol. 78, 573–590.

Hewson, R.D., Cudahy, T.J., Huntington, J.F., 2001. Geologic and alteration mapping at Mt Fitton, South Australia, using ASTER satellite-borne data. Int. Geosci. Remote Sens. Symp. 2, 724–726.

http://www.google.com/earth/index.html.

Hunt, G.R., 1977. Spectral signatures of particulate minerals in the visible and near infrared. Geophys. 42, 501–513.

Hunt, G.R., Salisbury, J.W., 1970. Visible and near infrared spectra of minerals and rocks: I. Silicate minerals. Mod. Geol. 1, 283–300.

Hunt, G.R., Salisbury, J.W., Lenhoff, C.J., 1971. Visible and near-infrared spectra of minerals and rocks: III Oxides and hydroxides. Mod. Geol. 2, 195–205.

Hunt, G.R., Salisbury, J.W., Lenhoff, C.J., 1974. Visible and near infrared spectra of minerals and rocks, IX, basic and ultrabasic igneous rocks. Mod. Geol. 5, 15–22.

Johnson, P.R., Kattan, F.H., Al-Saleh, A.M., 2004. Neoproterozoic ophiolites in the Arabian Shield: field relations and structure. In: Kusky, T.M. (Ed.), Precambrian Ophiolites and Related Rocks, vol. 13. Elsevier, Amsterdam, pp. 129–162.

Kruse, F.A., Lefkoff, A.B., Boardman, J.B., Heidebreicht, K.B., Shapiro, A.T., Barloon, P.J., Goetz, A.F.H., 1993. The Spectral Image Processing System (SIPS) interactive visualization and analysis of imaging spectrometer data. Remote Sens. Environ. 44, 145–163.

Kusky, T.M., Ramadan, T., 2002. Structural controls on NeoProterozoic mineralization in the SE Desert, Egypt: an integrated Field, Landsat TM, and SIR C/X APPROACH. J. Afr. Earth Sci. 35, 107–121.

Kusky, T.M., Robinson, C., El-Baz, F., 2005. Tertiary and Quaternary faulting and uplift of the Hajar Mountains of Northern Oman and the U.A.E. J. Geol. Soc. Lond. 162, 1–18.

Leblanc, M., Ceuleneer, G., 1992. Chromite crystallization in a multicellular magma flow: evidence from a chromitite dikes in the Oman ophiolite. Lithos 27, 231–257.

Li, J.H., Kusky, T.M., Huang, X., 2002. Neoarchean podiform chromitites and harzburgite tectonite in ophiolitic melange, North China Craton, remnants of Archean oceanic mantle. GSA Today 12 (7), 4–11.

Lippard, S.J., Shelton, A.W., Gass, I.G., 1986. The ophiolite of Northern Oman. Geological Society of London 11. Blackwell Scientific Publications, Oxford, U.K.

Loughlin, W.P., 1991. Principal component analysis for alteration mapping. Photogramm. Eng. Remote Sens. 57, 1163–1169.

Mars, J.C., Rowan, L.C., 2006. Regional mapping of phyllic- and argillic-altered rocks in the Zagros magmatic arc, Iran, using Advanced Spaceborne Thermal Emission and Reflection Radiometer (ASTER) data and logical operator algorithms. Geosphere 2 (3), 161–186.

Matthews, J.P., Jones, A.S.G., 1992. Mapping the Xigaze (Tibet) ophiolite complex with Landsat Thematic Mapper data. J. Himalayan Geol. 3, 97–101.

Moores, E.M., Robinson, P.T., Malpas, J., Xenophonotos, C., 1984. Model for the origin of the Troodos massif, Cyprus, and other Mideast ophiolites. Geology 12, 500–503.

Nicolas, A., Al Azri, H., 1991. Chromite-rich and chromite-poor ophiolites: the Oman case. Oman In: Peters, T., et al. (Ed.), In Ophiolite Genesis and Evolution of the Oceanic Lithosphere. Kluwer, Dordrecht, The Netherlands, pp. 261–274.

Nicolas, A., Prinzhofer, A., 1983. Cumulative or residual origin for the transition zone in ophiolites: structural evidence. J. Petrol. 24, 188–206.

Ninomiya, Y., Fu, B., Cudahy, T.J., 2005. Detecting lithology with Advanced Spaceborne Thermal Emission and Reflection Radiometer (ASTER) multispectral thermal infrared "radiance-at-sensor" data. Remote Sens. Environ. 99, 127–139.

Okada, K., Ishii, M., 1993. Mineral and lithological mapping using thermal infrared remotely sensed data from ASTER simulator. International Geosciences and Remote Sensing Symposium "Better Understanding of Earth Environment", 93, pp. 126–128.

Podwysockii, M.H., Segal, D.B., Abrams, M.J., 1983. Use of multispectral images for assessment of hydrothermal alteration in the Marysvale, Utah mining area. Econ. Geol. 78, 675–687.

Prichard, H.M., Lord, R.A., NEARY, C.R., 1996. A model to explain the occurrence of platinum- and palladium-rich ophiolite complexes. J. Geol. Soc. Lond. 153, 323–328.

Rajendran, S., Thirunavukkarasu, A., Balamurugan, G., Shankar, K., 2011. Discrimination of iron ore deposits of granulite terrain of Southern Peninsular India using ASTER data. J. Asian Earth Sci. 41, 99–106.

Ramadan, T.M., Abdelsalam, M.G., Stern, R.J., 2001. Mapping gold-bearing massive sulfide deposits in the Neoproterozoic Allaqi suture, SE Egypt with Landsat TM and SIR-C/X-SAR images. J. Photogramm. Eng. Remote Sens. 67, 491–497.

Richards, J.A., Xiuping, J., 1998. Remote Sensing Digital Image Analysis, Third ed. Springer, Berlin. p. 363.

Rokos, D., Argialas, D., Mavrantza, R., St.-Seymour, K., Vamvoukakis, C., Kouli, M., Lamera, S., Paraskevas, H., Karfakis, I., Denes, G., 2000. Structural mapping and analysis for a preliminary investigation of possible gold mineralization by using remote sensing and geochemical techniques in a GIS environment: study area: island of Lesvos, Aegean Sea, Hellas. Nat. Resour. Res. 9, 277–293.

Rothery, D.A., 1987a. Improved discrimination of rock units using Landsat Thematic Mapper imagery of the Oman ophiolite. J. Geol. Soc. Lond. 144, 587–597.

Rothery, D.A., 1987b. Decorrelation stretching a an aid to image interpretation. Int. J. Remote Sens. 8, 1253–1254.

Rowan, L.C., Mars, J.C., 2003. Lithologic mapping in the Mountain Pass, California area using Advanced Spaceborne Thermal Emission and Reflection Radiometer (ASTER) data. Remote Sens. Environ. 84, 350–366.

Rowan, L.C., Wetlaufer, P.H., Goetz, A.F.H., Billingsley, F.C., Stewart, J.H., 1974. Discrimination of rock types and detection of hydrothermally altered areas in south-central Nevada: U.S. Geol. Sur. Prof. Pap. 883, 35.

Rowan, L.C., Goetz, A.F.H., Ashley, R.P., 1977. Discrimination of hydrothermally altered rocks and unaltered rocks in visible and near infrared multispectral images: geophysics 42, 522–535.
Rowan, L., Hook, S.J., Abrams, M.J., Mars, J.C., 2003. Mapping hydrothermally altered rocks at Cuprite, Nevada, using the Advanced Spaceborne thermal emission and reflection radiometer (ASTER), a new satellite-imaging system. Econ. Geol. Bull. Soc. Econ. Geol. 98 (5), 1019–1027.
Sabins, F., 1997. Remote Sensing Principles and Interpretationthird ed. 494.
Sabins, F.F., 1999. Remote sensing for mineral exploration. Ore Geol. Rev. 14, 157–183.
Searle, M.P., Malpas, J., 1980. The structure and metamorphism of rocks beneath the Semail ophiolite of Oman and their significance in ophiolite obduction. Trans. R. Soc. Edinb.: Earth Sci. 71, 213–228.
Sultan, M., Arvidson, R.E., Sturchio, N.C., 1986. Mapping of serpentinites in the Eastern Desert of Egypt using Landsat Thematic Mapper data. Geology 14, 995–999.
Sultan, M., Arvidson, R.E., Sturchio, N.C., Guinnes, E.A., 1987. Lithologic mapping in arid regions with Landsat TM data: Meatiq dome, Egypt. Geol. Soc. Am. Bull. 99, 748–762.
Swayze, G.A., Clark, R.N., Goetz, A.F.H., Livo, K.E., Sutley, S.S., 1998. Using imaging spectroscopy to better understand the hydrothermal and tectonic history of the Cuprite mining district, Nevada. In: Green, R.O. (Ed.), Summaries of the 7th JPL Airborne Earth Science Workshop: Jet Propulsion Laboratory, Pasadena, California, JPL Publication 97–21 (1), pp. 383–384.
Velosky, J.C., Stern, R.J., Johnson, P.R., 2003. Geological control of massive sulfide mineralization in the Neoproterozoic Wadi Bidah shear zone, southwestern Saudi Arabia, inferences from orbital remote sensing and field studies. Precambrian Res. 123, 235–247.
Watts, K.F., 1990. Mesozoic carbonate slope facies marking the Arabian platform margin in Oman: depositional history, morphology and palaeogeography. In: Robertson, A.H.F., Searle, M.P., RaES, A.C. (Eds.), The Geology and Tectonics of the Oman Region: Geol. Soc. Spec. Publ., 49, pp. 139–159.
Yamaguchi, Y., Naito, C., 2003. Spectral indices for lithologic discrimination and mapping by using the ASTER SWIR bands. Int. J. Remote Sens. 24, 4311–4323.
Yamaguchi, Y., Kahle, A.B., Kawakami, T., Paniel, M., 1998. Overview of the advanced spaceborne thermal emission and reflection radiometer (ASTER). IEEE Trans. Geosci. Remote Sens. 36 (4), 1062–1071.